Proceedings of the Combustion Institute 41 (2025) 105866

Contents lists available at ScienceDirect

Proceedings of the Combustion Institute

journal homepage: www.elsevier.com/locate/proci

Experimental investigation of turbulent premixed H_2-jet flames at high exhaust gas recirculation

Maurus Bauer [a,*], Björn Stelzner [a], Peter Habisreuther [a], Michael Schneider [a], Christof Weis [b], Dimosthenis Trimis [a]

[a] Karlsruhe Institute of Technology (KIT), Engler-Bunte-Institute, Combustion Technology, Germany
[b] DVGW Research Center at Engler-Bunte-Institute of Karlsruhe Institute of Technology (KIT), Germany

ARTICLE INFO

Keywords:
Premixed
Turbulent hydrogen jet flame
High exhaust gas recirculation
Flame structure
NO_X emissions

ABSTRACT

This study presents an experimental investigation of a turbulent premixed hydrogen jet flame operating under high exhaust gas recirculation (EGR) rates. Experiments were conducted at a Reynolds number of 10 000, exploring flames ranging from pure H_2–air mixtures to cases with an EGR rate of 0.67. The flames were carefully adjusted to maintain similar laminar burning velocities, enabling consistent comparisons and revealing a systematic increase in the equivalence ratio (Φ) with higher EGR rates. These operating conditions were derived through a detailed 1D analysis of H_2–air–EGR laminar flames using comprehensive chemical kinetics, complemented with measurements of the laminar burning velocities of premixed H_2–air–EGR flames. The flow field of the model burner setup and nozzle design was characterized under both non-reactive and reactive conditions using particle image velocimetry (PIV). OH* chemiluminescence imaging did not reveal significant changes in the overall structure of the flame, even as the equivalence ratio varied from $\Phi = 0.4$ (pure H_2–air flame) to near-stoichiometric conditions ($\Phi = 0.77$). Selected cases were further investigated using OH planar laser-induced fluorescence (OH-LIF), offering detailed visualization of the flame structure and corroborating the observations from OH* chemiluminescence. NO_X emissions remained low across all investigated EGR rates, demonstrating robust emission control. These findings enhance the understanding of hydrogen combustion dynamics under high EGR conditions and provide valuable insights for developing low-emission, high-stability combustion strategies.

1. Introduction

As the decarbonization of the energy market progresses, the widespread availability of hydrogen is anticipated in the near future, with hydrogen playing an increasingly critical role in various end-use applications. In addition to the utilization of synthetic hydrocarbons derived from “green” hydrogen, the direct combustion of hydrogen as a carbon-free chemical energy carrier presents a promising solution for mitigating CO_2 emissions. Hydrogen, compared to conventional hydrocarbons, exhibits unique characteristics such as high burning velocity, broad ignition limits, and a low quenching distance. Its elevated diffusivity leads to short reaction zones and thermodiffusive flame instabilities.

Lean premixed H_2–air flames are prone to combustion instabilities, especially thermodiffusive instabilities, due to hydrogen’s low Lewis number [1]. These instabilities amplify flame front perturbations, resulting in increased flame speeds [2]. Burning velocities up to four times higher than the unstretched laminar value under ambient conditions have been reported [3]. In turbulent H_2–air flames, thermodiffusive effects similarly play a major role [4]. Comparable trends are also observed for turbulent premixed CH_4/H_2–air flames, where finer wrinkled structures arise not only from increased turbulence intensity but also from higher hydrogen fractions [5].

However, the addition of water affects the pronounced instabilities of pure hydrogen flames. The interaction of liquid water droplets with a turbulent premixed hydrogen flame was investigated numerically using DNS calculations in [6]. It was reported that non-unity Lewis numbers are less significant in strongly lean cases (e.g., $\Phi = 0.6$), and thus preferential diffusion effects are reduced. Similar findings were reported in a kinetic analysis of hydrogen/steam–air combustion [7]. In addition, a reduction in NO_X emissions by approximately 50 % under near-stoichiometric conditions and high water loading (10 % by mass) was observed compared to cases without added steam.

The laminar burning velocity of H_2–air mixtures containing varying amounts of steam (up to 50 %) was measured using a nozzle burner

* Corresponding author.
E-mail address: maurus.bauer@kit.edu (M. Bauer).

https://doi.org/10.1016/j.proci.2025.105866
Received 2 May 2025; Accepted 5 September 2025
Available online 4 October 2025

across a range of stoichiometries and diluent fractions [8,9]. It was shown that steam dilution significantly reduced the laminar burning velocity. However, in some cases, third-body reactions led to increased heat release in the preheat zone and, consequently, to higher temperatures in the flame's reaction zone — a mechanism that counteracts steam's physical effect of lowering the flame temperature [8]. Concetti et al. [7] reported similar findings regarding the influence of third-body reactions and the reduction of laminar burning velocity when steam is used to lower the maximum flame temperature.

Hydrogen can be combusted under non-premixed conditions in technical systems to enhance operational safety. However, this approach leads to locally elevated peak temperatures, which promote the formation of nitrogen oxides (NO_X). To enable safe and efficient hydrogen combustion, premixed operation is generally preferred, as it allows for better control of flame temperature and, consequently, lower emissions, facilitating cleaner combustion.

However, premixed hydrogen flames pose challenges with flame stabilization, primarily due to high burning velocities and the risk of flashback. One effective strategy to address these issues is exhaust gas recirculation (EGR), which helps moderate flame temperature, reducing thermal NO_X formation [6] and mitigating the high burning velocities [8] that contribute to flashback.

The scope of this work is to investigate how cold exhaust gas recirculation affects the stability and structure of hydrogen flames. By moderating the flame temperature, EGR offers insights into optimizing hydrogen combustion while minimizing pollutant emissions. Additionally, recirculating cooled exhaust gases into the inlet stream can mitigate flame instabilities and further stabilize combustion.

2. Numerical and experimental determination of laminar burning velocity with exhaust gas recirculation

The investigation of laminar burning velocity in this study is divided into numerical and experimental analyses. Numerically, 1D hydrogen flames are computed using various H_2 mechanisms [10–14] and simulated with ANSYS ChemkinPro 21. In the simulation setup shown in Figure S1 in the Supplementary Material, a hydrogen–air mixture, $\dot{m}_0$, with equivalence ratio Φ, pressure p, and temperature T_{in} is fed into a mixing unit. Simultaneously, an equilibrium calculation is performed to determine the equilibrium temperature, T_{eq}, for the same mixture. The resulting gas stream, $\dot{m}_1$, which is constrained to consist only of the main species H_2, O_2, N_2, and H_2O (pseudo-equilibrium), is then adjusted to match the inlet temperature T_{in} of the initial H_2–air mixture before being introduced into the mixing unit. The gas stream exiting the mixing unit is subsequently used in the 1D hydrogen flame simulations. The recirculation rate in this study is defined as follows:

$$\mathrm{EGR} = \frac{\dot{m}_1}{\dot{m}_0}. \tag{1}$$

Fig. 1 presents a representative example of simulated laminar burning velocities of H_2–air mixtures, determined using the Konnov 2019 mechanism [13], as a function of the equivalence ratio Φ and the exhaust gas recirculation rate EGR, at a pressure of $p = 1\,\mathrm{bar}$ and an inlet temperature of $T_{in} = 398\,\mathrm{K}$.

Experimentally, the laminar burning velocity in this study is determined using the heat-flux burner method (HFBM) [15,16]. As a characteristic physico-chemical property of a fuel–oxidizer mixture at a given temperature and pressure, the laminar burning velocity serves as an important benchmark for validating reaction mechanisms. While numerous studies on the laminar burning velocity of H_2–air mixtures exist – comprehensively summarized, for instance, by Konnov et al. [17] – and several investigations have also addressed H_2–air–steam mixtures [8,9,18,19], to the authors' knowledge, no comprehensive data are currently available for H_2–air–EGR mixtures. In this study, actual exhaust gas recirculation is simulated using a synthetic recirculate composed of O_2, N_2, and H_2O. The first two species, along with H_2 and

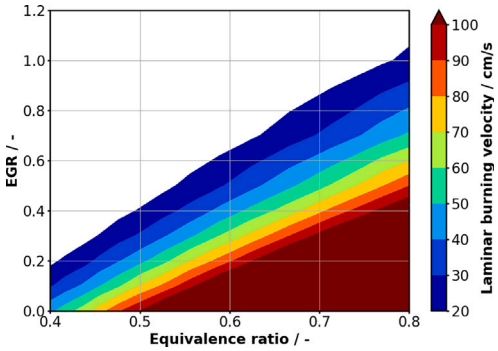

Fig. 1. Computed laminar burning velocities of H_2–air–EGR flames at $p = 1\,\mathrm{bar}$ and $T_{in} = 398\,\mathrm{K}$ using the Konnov 2019 mechanism [13].

air from the fresh gas mixture, are supplied to the burner via thermal mass flow controllers (MFCs), while deionized water is metered using a syringe pump and a low-pulsation direct evaporator. A description of the fundamental design of the heat-flux burner used in this study can be found in [20]. The application of the HFBM to lean H_2–air and H_2–air–EGR flames follows the approach described by Alekseev et al. [21] and requires extrapolating the laminar burning velocity from the subadiabatic region. Figs. 2 and 3 show the laminar burning velocities measured in this study using the HFBM, both with and without exhaust gas recirculation, for two representative measurement series. The experimental data are generally well reproduced by the simulation mechanisms. Although certain mechanisms may perform better in individual experiments, the ELTE mechanism [12] demonstrates the best overall agreement across all measurement series, exhibiting an average deviation of only 3.5 %.

The measured reduction in laminar burning velocity with increasing EGR is consistent with previous experimental studies on H_2–air–steam mixtures, which have reported a strong sensitivity of s_L to steam addition. The influence of water vapor can be attributed to three mechanisms – dilution, thermal, and chemical effects – that act simultaneously and are strongly interdependent, as described, for example, by Mazas et al. [22]. Several studies have highlighted the dominant role of the thermal effect, since water vapor acts as a thermal ballast due to its high specific heat capacity [18,23]. Chemical effects, however, have also been shown to play an important role: H_2O acts as an efficient third-body in recombination reactions and reduces the active radical pool [7,8,23,24]. At the same time, Koroll and Mulpuru [8], as well as Concetti et al. [7], have reported that, under certain conditions, third-body reactions involving H_2O can increase the flame speed and thereby partially counteract the thermal effect of steam dilution. The synthetic recirculate used in this study captures all of these effects simultaneously. An experimental isolation of the individual contributions has not been pursued here, as disentangling the mutually interacting effects would require a dedicated and complex experimental campaign that lies beyond the scope of this work.

3. Model burner — design and flow field characterization

The newly developed model burner in this project is schematically illustrated in Fig. 4. The burner consists of three concentrically arranged inlets to the combustion chamber: (1) the primary nozzle, through which a mixture of H_2, air, and recirculate flows into the combustion chamber; (2) the annular gap formed between the primary and secondary nozzle; and (3) a porous sintered plate that introduces the so-called co-flow. In this study, both the secondary flow and the co-flow are supplied with air. Mass flow controllers allow the independent regulation of the flow rates of individual species, enabling precise adjustment of the equivalence ratio and exhaust gas recirculation rate

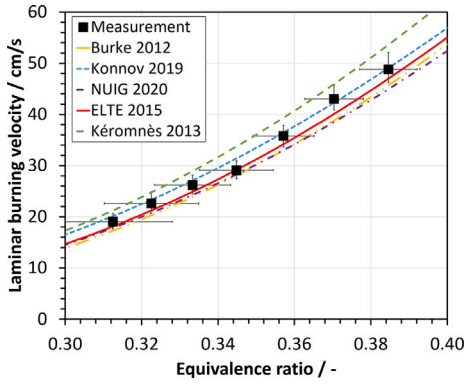

Fig. 2. Measured laminar burning velocities for pure H_2–air flames without EGR in comparison with simulation data of different H_2 mechanisms at p = 1 bar and T_{in} = 423 K.

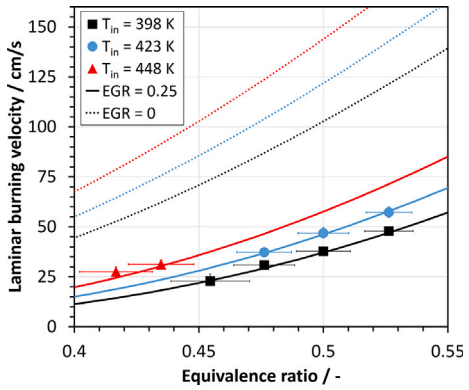

Fig. 3. Measured laminar burning velocities for H_2–air–EGR flames at EGR = 0.25, p = 1 bar and different preheat temperatures T_{in} in comparison with simulation data using the ELTE mechanism [12].

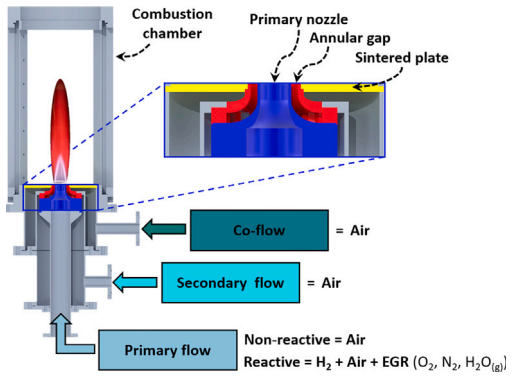

Fig. 4. Schematic representation of the model burner.

for the reactive experiments. For non-reactive experiments, the primary flow consists exclusively of air.

To ensure a comprehensive and systematic investigation of the processes occurring within the combustion chamber, an operating matrix is first established to facilitate stable and safe burner operation. In accordance with [25,26], two critical conditions are defined at the outlet of the primary nozzle: a minimum velocity gradient g_{min} to avoid flashback and a maximum velocity gradient g_{max} to prevent the flame from blowing off. Transferred to a Reynolds number at the nozzle outlet, this results in operating limits of Re_{min} = 2200 and Re_{max} = 20 000. To ensure safe operation, the Reynolds number of the primary nozzle is set to Re = 10 000 based on these values, and the operating matrix is created according to Table 1. The Reynolds number of the primary flow is defined using the nozzle diameter as the characteristic length, while for the secondary flow and the co-flow the hydraulic diameter of the annulus (i.e., twice the annular gap width) is used.

Table 1
Operating matrix of the model burner (Reynolds numbers at respective nozzle outlets).

Operating case	Primary flow Re	Secondary flow Re	Co-flow Re
1	10 000	10 000	1500
2	10 000	5000	1500

As a first step, the mixing concept is validated in non-reactive experiments. A nitrogen main flow is used, into which oxygen is injected at the position where hydrogen is introduced during reactive operation. The mixture subsequently passes through the static mixer (length 30 cm with structured packing material) and an additional 60 cm pipe section, which is deliberately included to provide extra residence time for mixing before the burner nozzle. At the burner nozzle outlet, the oxygen concentration of the nitrogen–oxygen mixture at ambient temperature (298 K) is measured using a paramagnetic analyzer (ABB Magnos28). The nozzle cross-section is scanned along two orthogonal centerlines in 1 mm increments with a sampling probe. At each position, 60 data points at 1 Hz are recorded after steady state is reached. The resulting oxygen concentrations are highly uniform, with a global mean of 10.9 %, a standard deviation of 0.11 %, and a maximum deviation from the mean of 0.28 %. Since hydrogen has a higher diffusivity than oxygen, its distribution after passing through the same mixing section can be expected to be at least as homogeneous. These results therefore confirm that the mixture at the burner outlet can be considered fully premixed.

In this study, two-dimensional velocity fields are experimentally determined using particle image velocimetry (PIV). As a light source for the PIV experiments, this study uses a frequency-doubled Nd:YLF double cavity laser (LitronLasers LDY304 PIV) with an emission wavelength of 527 nm. The laser beams, emitted with a time delay of Δt, are shaped into a laser light sheet with a height of 120 mm and directed through the center of the burner. The experiments are conducted with a repetition rate of 200 Hz. Scattered light is detected using a 12-bit CMOS camera (Vision Research Phantom v1212) with a resolution of 1280 x 800 pixels. A Nikon 50 mm f/1.4 lens is used for imaging. Commercial software (LaVision Davis 10) is utilized for image capture, parameter setting, perspective correction, and image correlation.

The time delay (Δt = 50 μs) between the double images is determined based on the size of the correlation window (24 x 24 pixels) and the velocity range of the experiment. The seeding material used in this study is DEHS (di-ethyl-hexyl sebacate) for the non-reactive experiments and the inert titanium dioxide (TiO_2) for the reactive operation of the burner. Fig. 5 shows the non-reactive velocity field, determined using PIV, for operating case 1 (see Table 1), where all flows are supplied with air (see Fig. 4). Shown here is the magnitude of the mean velocity $|u|$, normalized by the characteristic velocity u_c, which is defined as the theoretically calculated flow velocity at the outlet of the primary nozzle. The objective in developing the model burner was to generate a velocity profile over the primary nozzle that is as uniform and plug-shaped as possible. The background to this is that the high velocity gradients occurring with respect to the inner wall of the primary nozzle reduce the risk of flashback. Looking at Fig. 5, it is clear that the desired plug flow is actually present directly above the outlet of the primary nozzle. With increasing distance from the burner, the experimental results show a widening and increasingly homogenizing flow field.

The PIV images are also used to analyze the turbulence present in the combustion chamber and its intensity. Fig. 6 shows the turbulent

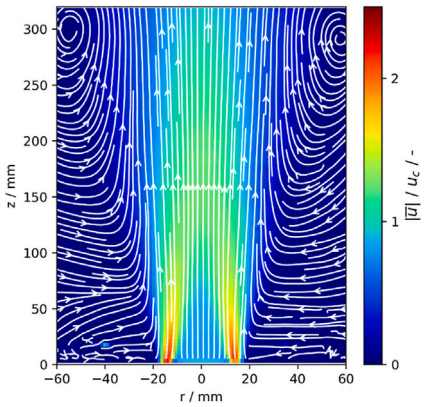

Fig. 5. Normalized mean velocities u for the non-reactive operating case 1 (see Table 1). The velocity u_c is defined as the velocity at the outlet of the primary nozzle.

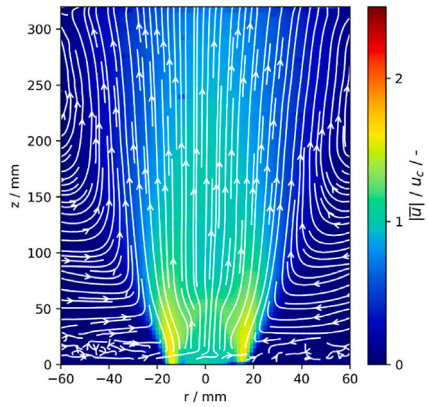

Fig. 7. Normalized mean velocities u for the reactive reference flame EGR = 0 and $\Phi = 0.5$ at operating case 1 (see Table 1). The velocity u_c is defined as the velocity at the outlet of the primary nozzle.

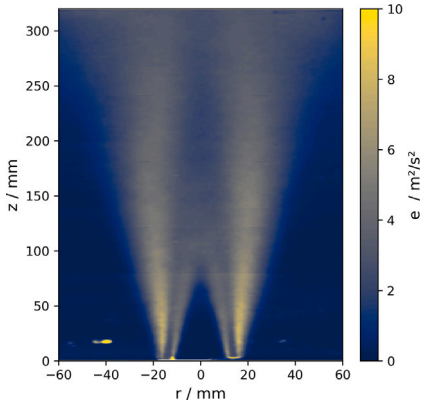

Fig. 6. Specific turbulent kinetic energy e for the non-reactive operating case 1 (see Table 1).

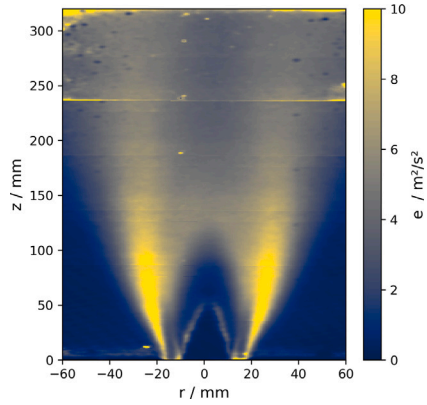

Fig. 8. Specific turbulent kinetic energy e for the reactive reference flame EGR = 0 and $\Phi = 0.5$ at operating case 1 (see Table 1).

kinetic energy e determined for operating case 1 (see Table 1), which is calculated according to [27,28] from the normalized variances in the axial $\left(\overline{u'_z u'_z}\right)$ and radial $\left(\overline{u'_r u'_r}\right)$ directions:

$$e = \frac{3}{4}\left(\overline{u'_z u'_z} + \overline{u'_r u'_r}\right). \tag{2}$$

The highest fluctuations occur in the region of the secondary flow, which forms shear layers with both the co-flow and the primary flow, leading to increased turbulence.

4. Characterization of the H_2 –air reference flames

After characterizing the burner under non-reactive conditions, the reactive flow field is analyzed under stable combustion conditions. A hydrogen–air flame with EGR = 0 and $\Phi = 0.5$ serves as the reference flame. At a preheat temperature of $T_{\text{in}} = 300\,\text{K}$, this flame exhibits a laminar burning velocity of $s_L \approx 50\,\text{cm}\,\text{s}^{-1}$, comparable to that of conventional hydrocarbon–air mixtures. This value is used as a reference condition to ensure consistent comparison across different flame configurations.

As observed in the description of the non-reactive flow field, the intended plug-shaped velocity profile is also evident directly at the exit of the primary nozzle. Fig. 7 further illustrates that the flow field is significantly influenced by the turbulent flame. In particular, the exothermic reaction at the flame front leads to an increase in gas velocity in both the axial and radial directions. As a result of these radial velocity components, the flow profile in the combustion chamber is broader in the reactive case compared to the non-reactive case (see Fig. 5). In the secondary nozzle region, the normalized velocity is lower in the reactive case compared to the non-reactive case. This is due to the presence of a hydrogen–air mixture in the reactive case, whereas only air flows through the primary and secondary nozzles in the non-reactive case. The two gas mixtures differ in density and kinematic viscosity. To maintain a constant Reynolds number, the velocity in the primary nozzle is adjusted, affecting the velocity ratio in the secondary nozzle relative to u_c.

Considering the turbulent kinetic energy in the reference flame's flow field (see Fig. 8), the highest fluctuations, similar to the non-reactive case (see Fig. 6), occur in the shear layers between the secondary flow, co-flow, and primary flow. However, Fig. 8 also reveals additional turbulence in the flame front region, induced by combustion reactions. In both non-reactive (see Fig. 6) and reactive cases (see Fig. 8), the turbulence intensity decreases with increasing distance z from the burner, as turbulent kinetic energy dissipates along the fluid flow.

To determine the operating limits of the developed model burner, the reference flame at $\Phi = 0.50$ serves as the starting point. From there, the equivalence ratio is gradually reduced while the flame structure is monitored via OH* chemiluminescence imaging. As an example, Figure S2 in the Supplementary Material shows averaged OH* images from an experimental series conducted at $T_{in} = 300\,\text{K}$ for operating case 1 (see Table 1), covering the range from $\Phi = 0.53$ to $\Phi = 0.29$. Notably, no flame lifting is observed down to $\Phi = 0.25$. Starting from the same reference flame at $\Phi = 0.50$, stable operation of the burner is also maintained as the equivalence ratio increases. No flashback occurs up

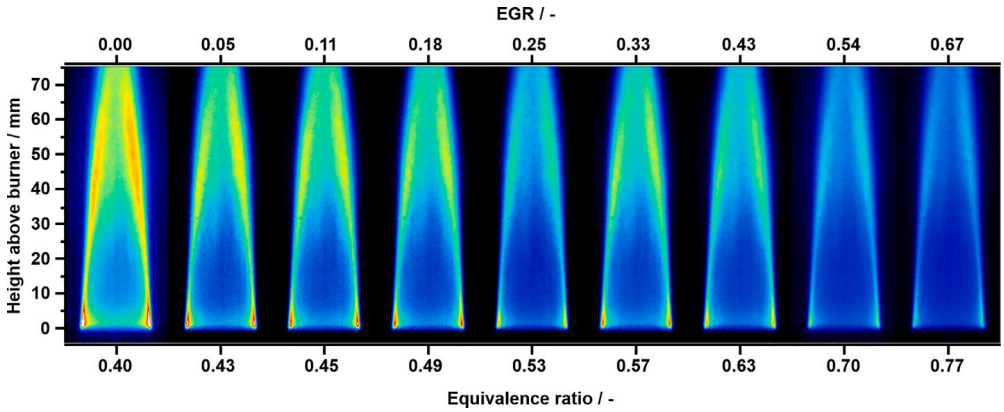

Fig. 9. OH* chemiluminescence images of hydrogen–air–EGR flames ($p = 1$ bar, $T_{in} = 398$ K, operating case 2 (see Table 1)) for an experimental series varying equivalence ratio and EGR at constant $s_L \approx 50\,\mathrm{cm\,s^{-1}}$.

to stoichiometric conditions ($\Phi = 1.0$), even at an elevated preheat temperature of $T_{in} = 398$ K.

5. H_2 –air–EGR flames — reaction zones and no_x emissions

For the investigation of H_2–air flames with exhaust gas recirculation, OH* images are taken to determine the flame's position and extent within the combustion chamber. The experimental series shown in Fig. 9 illustrates the chemiluminescence images obtained for varying equivalence ratio Φ and EGR at a reactant preheat temperature of $T_{in} = 398$ K for operating case 2 (see Table 1). Starting with a pure H_2–air flame (EGR = 0) at $\Phi = 0.4$, the equivalence ratio and recirculation rate are adjusted to maintain $s_L \approx 50\,\mathrm{cm\,s^{-1}}$ as the mixture composition approaches stoichiometry. This criterion is chosen to provide comparable flame anchoring conditions at the nozzle outlet across all operating points, which is particularly relevant for the technical application that motivated this study, namely infrared radiant tube heaters. The experimentally chosen operating conditions are based on the numerically determined relationship between recirculation rate, equivalence ratio, and flame speed (see Fig. 1). Fig. 9 shows that with a significant increase in equivalence ratio towards stoichiometry and simultaneous increase in EGR, the OH* radiation intensity decreases. However, the general flame structure remains intact. The experimental series also demonstrates that the thermal output of the flame changes by only about 7 % between the flame at $\Phi = 0.4$ and EGR = 0 and the flame at $\Phi = 0.77$ and EGR = 0.67, thus maintaining a nearly constant value of approximately 5 kW.

The determination of the reaction field in this study is carried out not only through the recording of OH* chemiluminescence but also through the detection of fluorescence radiation of the hydroxyl radical (OH) induced by laser excitation. This technique, known as OH-LIF (laser-induced fluorescence), involves OH radicals initially absorbing resonant laser radiation and then relaxing by releasing energy in the form of frequency-shifted radiation (fluorescence) to their ground state. Detailed information on laser-induced fluorescence and its application in combustion engineering can be found, for example, in [29]. In this study, a Sirah dye laser (Credo-Dye-N) operating with Rhodamine 6G as the dye is used. The laser beam, emitted at a wavelength of approximately 283 nm, is shaped into a laser light sheet, passes through the center of the combustion chamber, and excites OH radicals in the A-X transition at the $Q_1(6)$ rotational state. Signal detection occurs through the transitions (0,0) and (1,1). For data acquisition, an intensified 12-bit CMOS camera (Vision Research Phantom v1212) with a resolution of 1280 x 800 pixels is used. Fig. 10 shows averaged OH-LIF images from 200 individual frames at a capture frequency of 100 Hz. The two extreme cases from the experimental series, already discussed in Fig. 9 at $\Phi = 0.4$ and EGR = 0 as well as at $\Phi = 0.77$ and EGR = 0.67, are presented

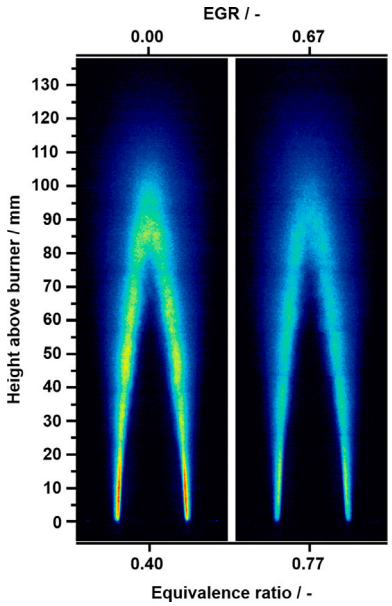

Fig. 10. OH-LIF images of hydrogen–air–EGR flames at constant $s_L \approx 50\,\mathrm{cm\,s^{-1}}$ ($p = 1$ bar, $T_{in} = 398$ K, operating case 2 (see Table 1)).

here. As observed in the OH* images, the averaged radiation intensity in the LIF images decreases with increasing equivalence ratio and EGR, while the flame structure and flame length remain similar. Unlike the OH* images, where the measurement signal is integrated over the entire flame, the OH-LIF images clearly show that the combustion reactions occur only within a spatially confined, cone-shaped region. Especially near the primary nozzle, the reaction zones shown in Fig. 10 are narrow, implying a nearly stationary flame position. With increasing distance from the burner, the region in which OH-LIF radiation is detected expands, which can be explained by the temporal and spatial fluctuations in flame shape and position. Superimposing the individual LIF images results in a flame zone typical of turbulent flames, often referred to as a "flame brush".

The reactive experiments are accompanied by measurements of the exhaust gas composition, with a particular focus on nitrogen oxide (NO_X) emissions. The exhaust gas is drawn globally at the outlet of the combustion chamber through a probe. The extracted sample is first passed through a gas cooler, where the water content in the exhaust gas is condensed. The dry exhaust gas is then directed through various analyzer modules. NO_X emissions are measured with a chemiluminescence detector (Eco Physics CLD700 EL), which employs two measurement

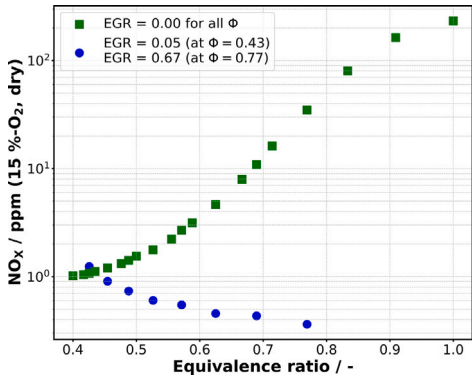

Fig. 11. Global NO_X concentrations of various test series standardized to 15 % O_2 in dry exhaust gas at $p = 1$ bar, $T_{in} = 398$ K, operating case 2 (see Table 1).

cells: one detecting NO directly, and the other detecting total NO_X (NO + NO_2) after catalytic conversion of NO_2 to NO upstream of the second cell. The O_2 concentration is determined using a paramagnetic analyzer (ABB Magnos28). Hydrogen conversion is monitored with a thermal conductivity detector (ABB Caldos27), which measures H_2 concentrations in vol.%. At each operating point, 60 exhaust gas measurements are recorded after reaching steady state, with a sampling frequency of 60 Hz. In addition, a high-sensitivity H_2 sensor with ppm-level detection capability is installed at the exhaust as part of the safety system. No residual hydrogen is detected in any experiment.

The resulting arithmetic mean values are shown in Fig. 11 for NO_X emissions. The measurements are normalized to an oxygen content of 15 % (volumetric) in the dry exhaust gas. The blue points in Fig. 11 represent NO_X measurements from the previously discussed experimental series, varying the equivalence ratio and EGR ($s_L \approx 50\,\mathrm{cm\,s^{-1}}$), and therefore correspond to the flames visualized in Figs. 9 and 10. It can be seen that starting from a measurement of approximately 1 ppm NO_X ($\Phi = 0.4$ and EGR = 0), the NO_X emissions decrease to about 0.4 ppm at $\Phi = 0.77$ and EGR = 0.67, representing a 60 % reduction in emission values.

A second experimental series, shown here as the green rectangle, starts from the same flame ($\Phi = 0.4$, EGR = 0, $T_{in} = 398$ K), with the equivalence ratio being increased towards stoichiometry, while the recirculation rate (EGR = 0) and preheat temperature ($T_{in} = 398$ K) remain constant. Compared to the blue data points, the average NO_X emissions initially increase slowly but then rise exponentially, reaching approximately 35 ppm at $\Phi = 0.77$ (EGR = 0). With a further increase in equivalence ratio, the measurements increase to about 232 ppm NO_X at $\Phi = 1.0$ (EGR = 0, $T_{in} = 398$ K). This significant difference in NO_X emissions between the two experimental series can be attributed to the exhaust gas recirculation. In the experiments without exhaust gas recirculation, the combustion temperature increases towards a stoichiometric mixture, favoring NO_X formation via the thermal NO_X formation mechanism prevalent in H_2 combustion. However, when the recirculation rate is increased, the recirculated exhaust gas acts as an additional thermal ballast, inhibiting NO_X formation.

6. Conclusion

The present study focuses on the investigation and development of a concept for the safe and low-emission combustion of premixed, turbulent H_2–air flames. The fundamental idea is to address the specific challenges of hydrogen combustion — such as high burning velocities, short reaction zones, and susceptibility to instabilities — by deliberately recirculating cooled exhaust gases. Such exhaust gas recirculation reduces flame temperature and nitrogen oxide emissions while simultaneously lowering the burning velocity of the H_2–air flame.

To experimentally investigate this combustion concept, a model burner is designed, constructed, and manufactured. The burner design is supported by parametric simulations of 1D H_2–air flames with exhaust gas recirculation, as well as by experimental determination of the laminar burning velocity using the heat-flux burner method. The non-reactive flow field inside the combustion chamber is analyzed using particle image velocimetry (PIV). The results confirm the intended plug-shaped velocity profile at the burner nozzle outlet, ensuring increased flashback resistance.

In reactive operation, the structure of H_2–air flames with exhaust gas recirculation is analyzed using PIV, OH* chemiluminescence imaging and laser-induced fluorescence of OH radicals (OH-LIF). Experiments are conducted under varying reactant preheat temperatures, equivalence ratios Φ, and recirculation rates. The results demonstrate that the developed model burner enables stable and safe combustion over a wide operating range, from lean mixture compositions ($\Phi = 0.25$) to stoichiometric conditions ($\Phi = 1$). Furthermore, the structure and position of the H_2–air flame remain stable even when the equivalence ratio is significantly raised in conjunction with an elevated recirculation rate. The accompanying analysis of the exhaust gas composition clearly shows that targeted recirculation of cooled exhaust gases significantly reduces nitrogen oxide emissions compared to pure H_2–air flames.

In summary, the present study demonstrates that the recirculation of cooled exhaust gases enables stable and low-emission combustion of premixed, turbulent H_2–air flames. The results confirm a significant reduction in nitrogen oxide emissions.

Novelty and significance statement

The novelty of this research lies in the development and experimental validation of a burner concept that enables stable, premixed hydrogen–air combustion through targeted recirculation of cooled exhaust gases.

It is significant because it addresses key challenges of hydrogen combustion — such as high burning velocities and NO_X formation — by enhancing flame stability. By employing a comprehensive multi-diagnostic approach, combining well-established optical techniques (OH* chemiluminescence, OH-LIF, PIV) with detailed 1D simulations of H_2–air–EGR laminar flames, the study provides new insight into flame stabilization and NO_X reduction under high-EGR conditions and demonstrates a robust strategy for achieving low-emission hydrogen combustion across a wide operating range.

CRediT authorship contribution statement

Maurus Bauer: Writing – review & editing, Writing – original draft, Visualization, Investigation, Formal analysis. **Björn Stelzner:** Writing – review & editing, Supervision, Conceptualization. **Peter Habisreuther:** Writing – review & editing, Software. **Michael Schneider:** Writing – review & editing, Investigation. **Christof Weis:** Writing – review & editing, Software. **Dimosthenis Trimis:** Writing – review & editing, Supervision, Project administration, Funding acquisition.

Declaration of competing interest

The authors declare that they have no known competing financial interests or personal relationships that could have appeared to influence the work reported in this paper.

Acknowledgments

The authors would like to acknowledge the financial support by the Friedrich and Elisabeth Boysen Foundation in the project “Premixed hydrogen combustion at high recirculation rates”, Germany (BOY-178) and from the Helmholtz Association, Germany’s MTET program, Resource and Energy Efficiency, Germany, Anthropogenic Carbon Cycle, Germany (38.05.01).

Appendix A. Supplementary data

Supplementary material related to this article can be found online at https://doi.org/10.1016/j.proci.2025.105866.

References

[1] S. Verhelst, T. Wallner, Hydrogen-fueled internal combustion engines, Prog. Energy Combust. Sci. 35 (6) (2009) 490–527.

[2] M. Matalon, C. Cui, J.K. Bechtold, Hydrodynamic theory of premixed flames: effects of stoichiometry and variable transport coefficients and arbitrary reaction orders, J. Fluid Mech. 487 (2003) 179–210.

[3] L. Berger, K. Kleinheinz, A. Attili, H. Pitsch, Characteristic patterns of thermodiffusively unstable premixed lean hydrogen flames, Proc. Combust. Inst. 37 (2) (2019) 1879–1886.

[4] J.B. Chen, H.G. Im, Stretch effects on the burning velocity of turbulent premixed hydrogen/air flames, Proc. Combust. Inst. 28 (1) (2000) 211–218.

[5] M. Zhang, M. Chang, J. Wang, Z. Huang, Flame dynamics analysis of highly hydrogen-enrichment premixed turbulent combustion, Int. J. Hydrog. Energy 45 (1) (2020) 1072–1083.

[6] R. Concetti, J. Hasslberger, N. Chakraborty, M. Klein, Effects of liquid water addition on turbulent premixed hydrogen/air combustion, Fuel 373 (2024) 132314.

[7] R. Concetti, J. Hasslberger, T. Sattelmayer, M. Klein, On the chemical effect of steam addition to premixed hydrogen flames with respect to NO_x emissions and flame speed, Flow, Turbul. Combust. 113 (2) (2024) 519–534.

[8] G. Koroll, S. Mulpuru, The effect of dilution with steam on the burning velocity and structure of premixed hydrogen flames, Symp. (International) Combust. 21 (1) (1988) 1811–1819.

[9] D. Liu, R. MacFarlane, Laminar burning velocities of hydrogen-air and hydrogen-air steam flames, Combust. Flame 49 (1) (1983) 59–71.

[10] M.P. Burke, M. Chaos, Y. Ju, F.L. Dryer, S.J. Klippenstein, Comprehensive H_2/O_2 kinetic model for high-pressure combustion, Int. J. Chem. Kinet. 44 (7) (2012) 444–474.

[11] A. Kéromnès, W.K. Metcalfe, K.A. Heufer, N. Donohoe, A.K. Das, C.-J. Sung, J. Herzler, C. Naumann, P. Griebel, O. Mathieu, M.C. Krejci, E.L. Petersen, W.J. Pitz, H.J. Curran, An experimental and detailed chemical kinetic modeling study of hydrogen and syngas mixture oxidation at elevated pressures, Combust. Flame 160 (6) (2013) 995–1011.

[12] T. Varga, T. Nagy, C. Olm, I. Zsély, R. Pálvölgyi, E. Valkó, G. Vincze, M. Cserháti, H. Curran, T. Turányi, Optimization of a hydrogen combustion mechanism using both direct and indirect measurements, Proc. Combust. Inst. 35 (1) (2015) 589–596.

[13] A.A. Konnov, Yet another kinetic mechanism for hydrogen combustion, Combust. Flame 203 (2019) 14–22.

[14] NUIGMech1.1, 2025, URL https://c3.universityofgalway.ie/combustionchemistrycentre/mechanismdownloads/.

[15] L.P.H. de Goey, A. van Maaren, R.M. Quax, Stabilization of adiabatic premixed laminar flames on a flat flame burner, Combust. Sci. Technol. 92 (1–3) (1993) 201–207.

[16] K.J. Bosschaart, Analysis of the Heat Flux Method for Measuring Burning Velocities (Ph.D. thesis), Eindhoven University of Technology, 2002.

[17] A.A. Konnov, A. Mohammad, V.R. Kishore, N.I. Kim, C. Prathap, S. Kumar, A comprehensive review of measurements and data analysis of laminar burning velocities for various fuel+air mixtures, Prog. Energy Combust. Sci. 68 (2018) 197–267.

[18] Y. Lyu, P. Qiu, L. Liu, C. Yang, S. Sun, Effects of steam dilution on laminar flame speeds of H_2/air/H_2O mixtures at atmospheric and elevated pressures, Int. J. Hydrog. Energy 43 (15) (2018) 7538–7549.

[19] N. Lamoureux, N. Djebaili-Chaumeix, C.E. Paillard, Laminar flame velocity determination for H_2-air-steam mixtures using the spherical bomb method, J. Phys. IV (Proceedings) 12 (7) (2002) 445–452.

[20] M.M. Sentko, S. Schulz, B. Stelzner, C. Anderlohr, M. Vicari, D. Trimis, Determination of temperature and water-concentration in fuel-rich oxy-fuel methane flames applying TDLAS, Combust. Flame 214 (2020) 336–345.

[21] V.A. Alekseev, M. Christensen, E. Berrocal, E.J. Nilsson, A.A. Konnov, Laminar premixed flat non-stretched lean flames of hydrogen in air, Combust. Flame 162 (10) (2015) 4063–4074.

[22] A. Mazas, B. Fiorina, D. Lacoste, T. Schuller, Effects of water vapor addition on the laminar burning velocity of oxygen-enriched methane flames, Combust. Flame 158 (12) (2011) 2428–2440.

[23] T. Le Cong, P. Dagaut, Experimental and detailed modeling study of the effect of water vapor on the kinetics of combustion of hydrogen and natural gas, impact on NO_x, Energy Fuels 23 (2) (2009) 725–734.

[24] J. Santner, F.L. Dryer, Y. Ju, The effects of water dilution on hydrogen, syngas, and ethylene flames at elevated pressure, Proc. Combust. Inst. 34 (1) (2013) 719–726.

[25] G. von Elbe, M. Mentser, Further studies of the structure and stability of burner flames, J. Chem. Phys. 13 (2) (1945) 89–100.

[26] B. Lewis, G. von Elbe, Combustion, Flames and Explosions of Gases, third ed., Academic Press, 1987.

[27] D.X. Ye, X.D. Lai, H. Li, PIV measurement and study on turbulence generator flow field of medium consistency pump, IOP Conf. Ser.: Earth Environ. Sci. 163 (1) (2018) 012120.

[28] C. Verwey, M. Birouk, Dissipation rate estimation in a highly turbulent isotropic flow using 2D-PIV, Flow Turbul. Combust. 109 (3) (2022) 647–665.

[29] J.W. Daily, Laser induced fluorescence spectroscopy in flames, Prog. Energy Combust. Sci. 23 (2) (1997) 133–199.